LOGIC
Journal of Engineering Design and Technology
Vol. 25 No.3 November; p. 201-209

p-ISSN : 1412-114X
e-ISSN : 2580-5649
http://ojs2.pnb.ac.id/index.php/LOGIC

COMPREHENSIVE ANALYSIS ON THE INFLUENCE OF FLAP WIDTH ON THE HYDRODYNAMIC PARAMETERS OF OWSC DEVICES

Rasya Aulia Nathania Nisa[1)], James Julian[1)*], Fitri Wahyuni[1)], Riki Hendra Purba[1)], Fathin Muhammad Mahdhudhu[2)], Elvi Armadani[3)]

1) Department of Mechanical Engineering, Universitas Pembangunan Nasional Veteran Jakarta, Jakarta, Indonesia
2) Department of Naval Architecture, Universitas Pembangunan Nasional Veteran Jakarta, Jakarta, Indonesia
3) Department of Industrial Engineering, Universitas Pembangunan Nasional Veteran Jakarta, Jakarta, Indonesia

Corresponding email [1)] : zames@upnvj.ac.id

Abstract. The growing need for renewable energy has driven significant interest in harnessing ocean wave power, particularly through Oscillating Wave Surge Converters (OWSCs). This study focuses on examining the effect of flap width on the hydrodynamic capacity of an OWSC, as flap geometry plays a crucial role in energy capture efficiency. A numerical methodology utilizing the Boundary Element Method (BEM) was employed to assess hydrodynamic parameters across both temporal and frequency domains. Five flap width variations were tested under regular wave conditions with different periods, while mesh independence and validation against experimental data ensured accuracy. The results in the time domain revealed a direct correlation between flap width and angular deviation, velocity, torque, and power output, although wider flaps exhibited less stability due to increased inertia. Frequency domain analysis indicated that each flap width had a distinct resonant peak, with narrower flaps performing best at shorter periods and wider flaps at longer ones. Notably, moderately sized flaps (W2 and W3) achieved the highest efficiency, with Capture Width Ratios exceeding 70%, outperforming wider flaps despite their larger surface area. These findings highlight the importance of optimized flap width for efficient and reliable OWSC design.

Keywords: Flap Width, Hydrodynamic, OWSC, Time Domain, Wave Energy.

1. INTRODUCTION

The global energy sector faces critical challenges due to its reliance on finite and environmentally damaging non-renewable sources, which contribute to climate change and geopolitical instability. This pushes for a diversification into renewable energy technologies [1], [2]. Ocean wave energy, presenting a substantial and largely unexplored source for clean power generation, is estimated to have a global potential of 2 TW [3], [4], [5]. The core challenge lies in developing efficient and cost-effective devices, known as Wave Energy Converters (WECs), to harness this mechanical energy. One effective WEC design is the Oscillating Wave Surge Converter (OWSC), which typically employs a hinged flap responding to the horizontal surge motion of waves to drive a Power Take-Off (PTO) system, converting the mechanical energy into electricity [6]. OWSCs are generally preferred for deployment in nearshore environments due to their accessibility, design simplicity, and high efficiency in capturing energy [7]. These features have made OWSC devices the focus of many studies, many of which focus on enhancing the performance of the device.

Various studies have shown that multiple design parameters, including the size, shape, and submergence of the flap, influence the performance of an OWSC. One study by Lin et. al analyzes the effect of plate geometry parameters such as width, thickness, cross-section, and number of segments on the performance of an OWSC. The study concluded that cross cross-section and width of the plate have a distinct influence on its performance [8]. Nevertheless, this study does not provide a detailed analysis of the hydrodynamic characteristics of the device. Another study by Cui et. al investigates the effect of cross-sectional shapes of the flap on the performance of the device, which resulted in the rectangular shape as the best configuration for capturing energy [7]. However, this study is limited to 2D cases, so it does not consider the width or volume of the flap. Furthermore, a study by Anggara et. al further highlights that the dimensional parameters, namely the ratio of width to thickness, of the

flap govern the performance of the device [9]. Nonetheless, as this study investigates the ratio of two dimensions where one dimension is constrained by the other, it does not give an analysis of the individual dimensions of the flap. Although a study by Wang et al. [10] examined the effect of flap width on an OWSC's performance, it concentrated solely on the frequency domain hydrodynamic parameters.

From the previous studies, it can be inferred that flap dimensions influence the energy capture of the wave. However, these studies lack detailed, hydrodynamic investigations on the effect of specific and individual dimensions of the flap. Therefore, the main objective of this study is to investigate the effect of flap width on the flap hydrodynamic parameters of an OWSC. Furthermore, this study offers a novelty by providing an analysis of both the frequency domain and time domain, allowing for a detailed understanding of these parameters. This is crucial for optimizing the design to produce stable and consistent power output, which is essential for integration into the electrical grid. Additionally, time-domain hydrodynamic parameters will provide valuable insights into how to fine-tune OWSC designs to maximize power generation, thereby contributing to the development of a more reliable and efficient wave energy sector.

2. METHODS

2.1 Design of the Variations

This research investigates the hydrodynamic parameters of various widths on an OWSC. The selection of these flap dimensions was based on the dimensions of the experimental prototype by Wei et al (shown by W3 variation), which then the width variations are selected with a difference of 0.2 m. This technology is a type of WEC that harvests the surging kinetic energy of waves using a hinged flap. As a response to the surging wave, the flap will oscillate and then transfer the energy to a hydraulic power system [6]. This study's geometry is based on the model employed in an experimental investigation by Wei et al. [11]. This is carried out because the model is sufficiently compatible to be computed using the numerical approach used in this study, in addition to serving as a validation reference to preserve data actualization. As seen in Figure 1, five width variations are examined while maintaining constant thickness, height, and water depth. The dimension of each variation is shown in Table 1.

Table 1. Flap Dimensions of Each Variation.

Variations	Height (m)	Width (m)	Thickness (m)	Mass (kg)	Water Depth (m)
W1		0.4		2.662	
W2		0.6		4.299	
W3	0.31	0.8	0.0875	5.323	0.305
W4		1		6.654	
W5		1.2		7.985	

2.2 Governing Equations

The Boundary Element Method (BEM) is employed in this study, which involves several equations. The foundation of BEM for wave-body interaction problems is potential flow theory, which makes the assumptions that the fluid is irrotational, inviscid, and incompressible [12]. This method uses Laplace and Bernoulli equations to calculate the forces and torques exerted on the OWSC flap. The linear potential flow theory is crucial for calculating wave forces, with Eq 1 representing the flow field's velocity potential [8]. Eq 2 describes the hydrodynamic characteristics of the flap as a single body in the frequency domain, which includes the added mass matrix, damping matrix, mass matrix, as well as the wave exciting force. The flap's response to a specific wave force with a constant amplitude is calculated with Eq 3 in the time domain [8].

$$\nabla^2\phi(x,y,z,t) = \phi_I(x,y,z,t) + \phi_D(x,y,z,t) + \phi_R(x,y,z,t) = a_w\varphi(x,y,z,t)e^{-i\omega t} \quad (1)$$

$$M\ddot{X}(t) + K\dot{X}(t) + C_h X(t) = F(t) \quad (2)$$

$$\left[-\omega^2 (M_s + M_a(\omega)) - i\omega C(\omega) + K\right] X(\omega) = F(\omega) \quad (3)$$

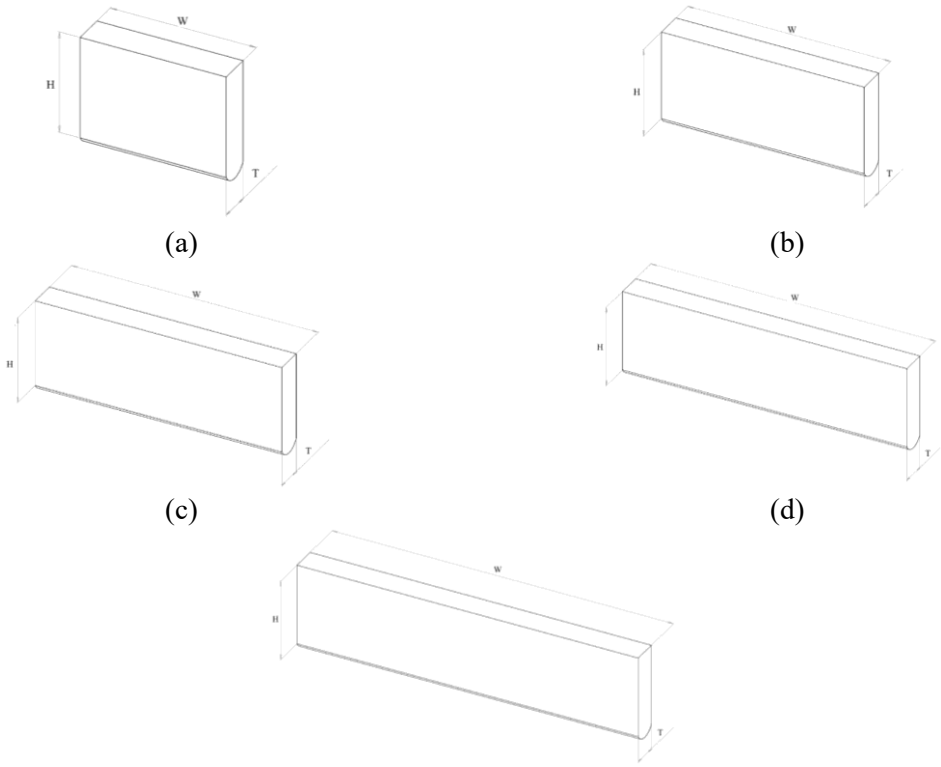

Figure 1. Geometry of width variations used in this study: (a) geometry of width 1 (W1), (b) geometry of width (W2), (c) geometry of width 3 (W3), (d) geometry of width 4 (W4), (e) geometry of width 5 (W5).

2.3 Mesh and Boundary Condition

The meshing process involves dividing geometry into smaller elements, allowing the equations within them to be solved. The preservation of mesh quality is paramount, as it significantly affects the accuracy, convergence, and stability of simulation outcomes. This study employs a quadrilateral mesh, segmenting the flap shape into smaller quadrilateral elements based on the surface domain. Figure 2 presents the mesh configuration.

Figure 2. Mesh configuration of the study.

Boundary conditions are also set up to simulate the actual interaction between the flap structure and ocean waves. This study employs a model of waves, which falls under the category of regular waves characterized by a constant amplitude. The ocean wave is modelled using the Airy Wave Theory [12] represented in Eq 4. An analysis of the device's hydrodynamic properties under different wave periods is done with the period variation listed in Table 2.

$$\eta(x,t) = \frac{h}{2}\cos(\omega t - k(x\cos\theta)) \quad (4)$$

Table 2. Ocean wave period variations.

Wave Configuration		
Amplitude (m)	Period (s)	Wavelength (m)
0.1	1.1	1.581
	1.3	1.975
	1.5	2.357
	1.7	2.730
	1.9	3.098
	2.1	3.462
	2.3	3.823
	2.5	4.181
	2.7	4.538
	2.9	4.893

Response data from the interaction between the ocean wave and the OWSC device are analyzed to assess its hydrodynamic properties. Conversely, the device's hydrodynamic performance is achieved by examining several power statistics, including the mechanical power of the device and the power of the wave energy source, which are determined by Eqs (5) and (7), respectively [13]. Eq (6) describes the wave's group velocity, which is used to calculate the power of the wave energy source. Moreover, Eq (8), which also characterizes the device's efficiency, uses the capture width ratio (CWR) equation to determine the device's capacity to capture power.

$$P_w = \frac{1}{2}\rho g A^2 C_g \tag{5}$$

$$C_g = \frac{1}{2} C_p \left\{1 + \frac{kD}{\sinh kD \times \cosh kD}\right\} \tag{6}$$

$$P_{OWSC} = |\, \tau(t) \times \omega(t) \,| \tag{7}$$

$$CWR = \frac{P_{OWSC}}{P_w \times Width} \tag{8}$$

2.4 Mesh Independence Test

This study conducted a grid independence evaluation to examine numerical errors and ensure the model's accuracy. This study adopts the approach introduced by Roache [14]. Three mesh configurations were tested: coarse (13,352 elements), medium (20,642 elements), and fine (30,462 elements), with the number of elements constrained by a specific grid refinement ratio constrained by Eq (9). For each mesh, the maximum absolute amplitude is sampled at a wave amplitude of 0.1 meters and a period of 1.9 seconds. The order of accuracy is determined using Eq (10). The Grid Convergence Index (GCI) evaluates mesh accuracy using two forms: GCI_{fine}, which measures the error between medium and fine meshes, and GCI_{coarse}, which assesses the error between medium and coarse meshes. GCI_{fine} and GCI_{coarse} are formulated in Eq (11) and (12), respectively. To ensure error accuracy, calculations are performed within the convergence region, validated by Eq (14). The final error value for each mesh was then derived from Eq (15). Table 3 presents the results of the mesh independence test. In this table, the maximum response data was taken as sample data from each mesh variation. It can be seen that the variations achieved a convergence index of 1, which is within the convergence region, thus ensuring the accuracy of the error. The result demonstrates that the fine mesh configuration produces the lowest error. Accordingly, this configuration is selected for the study.

$$r = \frac{h_2}{h_1} \tag{9}$$

$$\bar{p} = \frac{\ln\left(\frac{f_3 - f_2}{f_2 - f_1}\right)}{\ln(r)} \quad (10)$$

$$GCI_{fine} = \frac{F_s\,|\epsilon|}{(r^{\bar{p}} - 1)} \quad (11)$$

$$GCI_{coarse} = \frac{F_s\,|\epsilon|\,r^{\bar{p}}}{(r^{\bar{p}} - 1)} \quad (12)$$

$$\epsilon = \frac{f_{n+1} - f_n}{f_n} \quad (13)$$

$$\frac{GCI_{fine}}{GCI_{coarse}\,r^{\bar{p}}} \approx 1 \quad (14)$$

$$fr_{h=0} = f_1 + \frac{(f_1 - f_2)}{(r^{\bar{p}} - 1)} \quad (15)$$

Table 3. Result of Mesh Independence Test.

Mesh Category	Fine	Medium	Coarse
Maximum Response (m)	57.63967514	57.64332581	57.64648465
$\bar{p}$		0.356885866	
r		1.5	
GCI_{fine}		0.044%	
GCI_{coarse}		0.0508%	
$\frac{GCI_{fine}}{GCI_{coarse}}$		1.000	
$f_{rh}=0$		57.66677285	
Error	0.03518%	0.04066%	0.04699%

3. RESULTS AND DISCUSSION

3.1 Data Validation

To ensure data actualization, data validation analysis was conducted before discussing the main data of the study. This analysis is executed by comparing the flap motion response data obtained through numerical methods with experimental data provided by Wei et. al [11]. This data is taken at a wave parameter of A=0.1m and T=1.9s. Figure 3 shows the comparison between numerical and experimental data. As depicted in the graph, the simulation data closely align with the experimental data points. The two datasets exhibit a high degree of similarity in terms of both frequency and phase angle. While minor variations in the amplitude are present (namely, 6% difference), the overall pattern and trend of the motion response are consistent, confirming the reliability of the numerical approach.

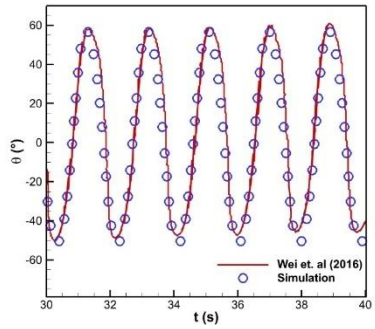

Figure 3. Comparison of experimental and simulation results for motion response at an ocean wave period of 1.9 seconds and an amplitude of 0.1 meters.

3.2 Data Analysis

The first set of data discussed is the hydrodynamic data in the time domain, subjecting the flaps to a wave with a period of 1.3 s and an amplitude of 0.1 m. Figure 4 depicts the motion response of each flap width variation over 40 seconds, showing that the motion for all five configurations is highly periodic and synchronous. A distinct and steady correlation exists between the width of the flap and the degree of angular deviation. As the flap width expands from W1 to W5, the degree of oscillation likewise rises. The widest flap, W5, achieves the largest angular deviation, while the narrowest, W1, has the smallest. This positive correlation occurs because a wider flap presents a larger surface area to the incoming waves, enabling it to absorb more energy. This results in a greater excitation force absorbed and, subsequently, a larger angular displacement.

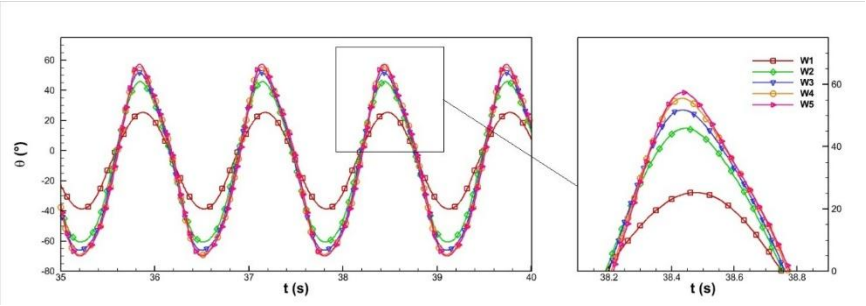

Figure 4. Motion response data of all variations when subjected to an ocean wave with a period of 1.3 seconds and an amplitude of 0.1 meters.

The hydrodynamic analysis reveals a clear proportionality between flap width and energy output parameters, despite the influence of inertial damping. Angular velocity, as shown in Figure 5 (a), is proportional to flap width because wider flaps capture a greater excitation force from the wave, resulting in higher absolute maximum angular velocity. The collateral increase in mass with width increases the inertial force, which acts as a damping force resisting motion, leading to less stable peak-to-trough transitions and greater hydrodynamic nonlinearity in wider flaps [15]. The torque, presented in Figure 5 (b), mirrors this proportionality, showing increased absolute maximum torque with wider flaps and similar trends in stability. An expected phase difference between torque and angular velocity exists, as torque functions as a restoring force opposing acceleration. Consequently, the device's power output, shown in Figure 5 (c) as the absolute product of torque and angular velocity, follows the same pattern: the wider the flap, the higher the power output. This consistently demonstrates that the influence of the absorbed excitation force significantly outweighs the inertial damping effect.

(a)

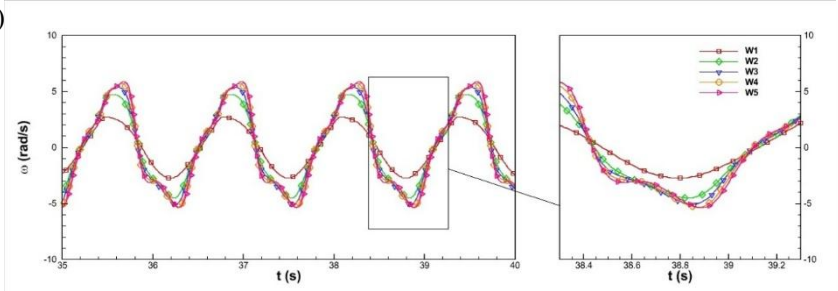

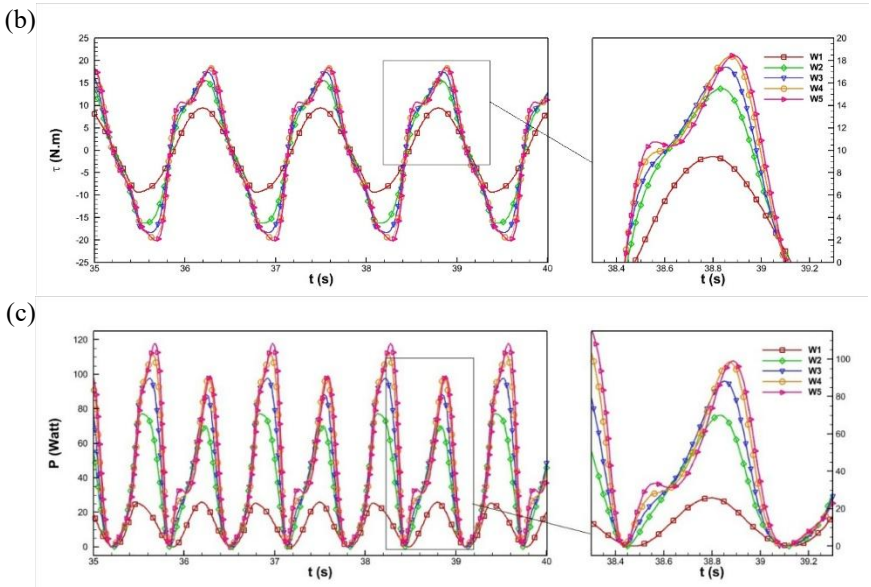

Figure 5. Other hydrodynamic parameters at ocean wave configuration of T=1.3 s and A=0.1 m, (a) angular velocity, (b) torque, and (c) power output.

The analysis of hydrodynamic parameters in the frequency domain reveals a strong dependence on both flap width and wave period across all variations. Figure 6 (a) illustrates that wider flaps (W2-W5) consistently achieve larger maximum angular deviations (motion response) for any given wave period, demonstrating their enhanced capacity for wave energy capture. The peaks across all variations in the maximum response data can be inferred as resonant peaks, which occur when the natural period of the structure aligns with the period of the wave, thus maximizing the motion of the structure [16]. The narrowest flap (W1) peaked sharply at approximately 1.1 seconds, while the wider flaps (W2-W5) are tuned to perform optimally in the longer period range of 1.3 to 1.5 seconds. This resonance phenomenon and the proportional relationship between flap width and performance are consistently reflected in the average angular velocity, average torque, and average power data shown in Figures 6 (b), (c), and (d). For instance, the maximum values for these parameters occur around 1.3 seconds for the wider flaps and 1.1 seconds for the narrowest flap, confirming that the substantial energy absorbed by wider flaps translates into a greater driving force, resulting in higher angular velocity, torque, and power despite traveling a greater angular distance.

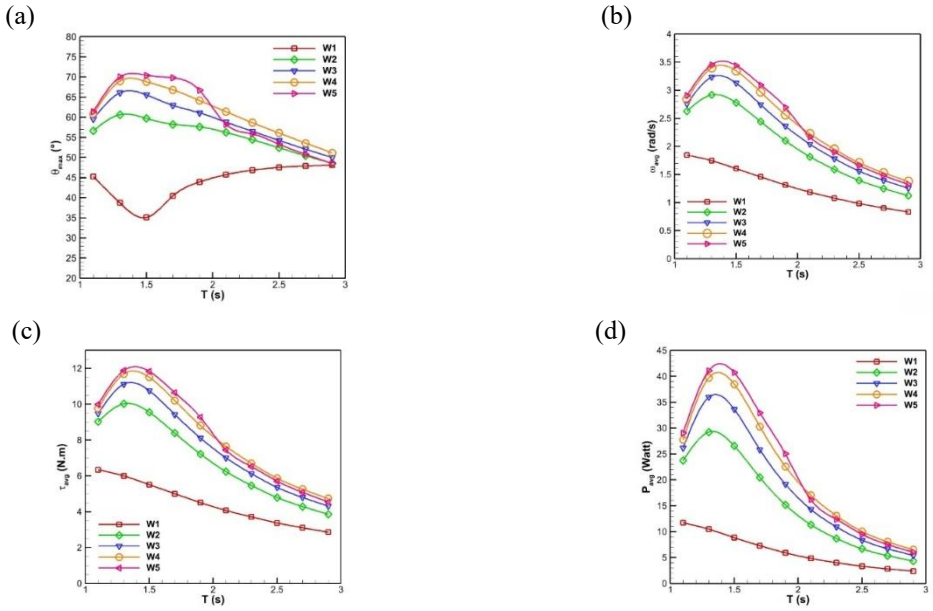

Figure 6. Hydrodynamic parameters at various ocean wave periods, (a) maximum response, (b) average angular velocity, (c) average torque, and (d) average power.

In the context of efficiency, it is formulated by the CWR data shown in Table 4. The data reveal a clear relationship between wave period and CWR, with an optimal performance zone for each flap width. As the wave period increases, the CWR for all configurations generally decreases after reaching a peak. The narrowest flap, W1, achieves its highest efficiency at the shortest wave period of around 1.1 s, with a CWR of 45.74%. However, the medium-width flaps (W2 and W3) demonstrate superior performance; they reached their peak efficiencies at a slightly longer period of around 1.3 s, with CWR values of 70.77% and 70.29%, respectively. The CWR for the widest flaps, W4 and W5, peaks at around 1.3 s, but at lower values of 62.08% and 53.50%, respectively. Beyond this optimal period, the efficiency for all flaps drops significantly. For instance, at 2.9 s, the CWR for all configurations falls below 11%. The data suggest that while wider flaps (W4 and W5) are effective at capturing a large wave front, their increased mass and hydrodynamic resistance might reduce their overall CWR compared to moderately-sized flaps (W2 and W3), especially in the optimal wave period range. This indicates that there is an optimal flap width that balances wave capture efficiency and hydrodynamic resistance to maximize the CWR. It can be noted that the current study achieved a higher maximum efficiency of 70.77% compared to other studies, which reach a maximum efficiency of around 50% [9], [10]

Table 4. Efficiency of the Flap Variations at Different Wave Periods.

Period (s)	Capture Width Ratio				
	W1	W2	W3	W4	W5
1.1	45.74%	57.45%	51.13%	43.38%	37.85%
1.3	40.96%	70.77%	70.29%	62.08%	53.50%
1.5	34.57%	64.29%	65.75%	60.16%	53.05%
1.7	26.79%	46.55%	47.47%	44.51%	40.33%
1.9	20.81%	33.04%	33.69%	31.76%	29.33%
2.1	16.45%	23.90%	24.35%	23.18%	18.35%
2.3	13.31%	17.90%	18.15%	17.38%	13.70%
2.5	10.84%	13.52%	13.66%	13.11%	10.33%
2.7	9.03%	10.69%	10.79%	10.35%	8.07%
2.9	7.58%	8.54%	8.63%	8.30%	6.39%

4. CONCLUSION

Using the Boundary Element Method (BEM), this study confirmed that flap width is a critical design parameter for the Oscillating Wave Surge Converter (OWSC), directly impacting energy capture and power output. In the time domain, increasing flap width led to proportional increases in motion response, angular velocity, torque, and power due to greater wave energy absorption and a stronger excitation force. However, increased inertia introduced a damping effect, causing less stable peak-to-trough transitions. In the frequency domain, each flap width exhibited a specific resonant peak (W1 at around 1.1 s; W2-W5 at around 1.3-1.5 s), but optimal efficiency was found in the moderately sized flaps (W2 and W3). The configurations achieved the highest Capture Width Ratio (CWR) values of 70.766% and 70.289%, respectively. When designing OWSC flaps, there should be a balance between wave capture against the dampening effects of inertia and hydrodynamic resistance, as moderately sized flaps (W2 and W3) achieved the highest efficiencies, outperforming wider flaps. Additionally, the frequency domain analysis guides designers to tune the flap's performance to the local wave climate: narrower flaps (W1) resonate best at shorter wave periods (around 1.1 s), while wider flaps (W2-W5) perform optimally at longer periods (around 1.3-1.5 s). This suggests that simply widening the flap does not guarantee maximum efficiency due to the adverse effects of added mass and hydrodynamic resistance, underscoring the need for future research with a finer resolution of wave periods to pinpoint the optimal design for specific wave climates.

6. REFERENCES

[1] Intergovernmental Panel on Climate Change (IPCC), “Climate Change 2022 - Mitigation of Climate Change: Working Group III Contribution to the Sixth Assessment Report of the Intergovernmental Panel on Climate Change,” *Cambridge University Press*, Jul. 2023, doi: doi.org/10.1017/9781009157926.

[2] IRENA, *Renewable Capacity Statistics 2025* . Abu Dhabi: International Renewable Energy Agency, 2025.

[3] W. R. Sari, G. Gunawan, A. Surjosatyo, D. Angga, and F. Muzhoffar, “Systematic Analysis of Potential Marine Renewable Energy for Coastal Ecological Balance on Bawean Island: A Review,” *International Journal of Marine Engineering Innovation and Research*, vol. 9, no. 2, pp. 1479–2548, Jun. 2024, doi: 10.12962/J25481479.V9I2.20298.

[4] A. Shadmani, M. R. Nikoo, A. H. Gandomi, M. Chen, and R. Nazari, "Advancements in optimizing wave energy converter geometry utilizing metaheuristic algorithms," *Renewable and Sustainable Energy Reviews*, vol. 197, p. 114398, Jun. 2024, doi: 10.1016/J.RSER.2024.114398.

[5] B. Yang *et al.*, "Wave energy converter array layout optimization: A critical and comprehensive overview," *Renewable and Sustainable Energy Reviews*, vol. 167, p. 112668, Oct. 2022, doi: 10.1016/J.RSER.2022.112668.

[6] W. A. Arrosyid *et al.*, "Recent advancements in wave energy converter technologies: A comprehensive review on design and performance optimization," *Ocean Engineering*, vol. 340, p. 122328, Nov. 2025, doi: 10.1016/J.OCEANENG.2025.122328.

[7] J. Cui, X. Chen, and S. Dai, "Numerical study on dual oscillating wave surge converter with different cross-section shapes using SPH under regular waves," *Ocean Engineering*, vol. 271, p. 113755, Mar. 2023, doi: 10.1016/J.OCEANENG.2023.113755.

[8] Y. Lin and F. Pei, "Numerical study on bottom-hinged plate wave energy converter geometry design," *Ocean Engineering*, vol. 260, Sep. 2022, doi: 10.1016/j.oceaneng.2022.112050.

[9] R. A. Anggara, J. Julian, F. Wahyuni, R. H. Purba, and N. T. Bunga, "Investigation of Flap Dimensional Parameters to Improve Hydrodynamic Performance of Oscillating Wave Surge Converter Device," *Jurnal Asiimetrik: Jurnal Ilmiah Rekayasa & Inovasi*, vol. 7, no. 1, pp. 59–70, Jan. 2025, doi: 10.35814/ASIIMETRIK.V7I1.7911.

[10] D. Wang, S. Qiu, and J. Ye, "Width effects on hydrodynamics of pendulum wave energy converter," *Applied Mathematics and Mechanics (English Edition)*, vol. 35, no. 9, pp. 1167–1176, Sep. 2014, doi: 10.1007/s10483-014-1857-6.

[11] Y. Wei, T. Abadie, A. Henry, and F. Dias, "Wave interaction with an Oscillating Wave Surge Converter. Part II: Slamming," *Ocean Engineering*, vol. 113, pp. 319–334, Feb. 2016, doi: 10.1016/j.oceaneng.2015.12.041.

[12] J. N. Newman, "Marine Hydrodynamics, 40th edition," *The MIT Press Cambridge, Massachusetts London, England*, p. 450, 2018, Accessed: Aug. 18, 2025. [Online]. Available: https://mitpress.mit.edu/9780262534826/marine-hydrodynamics/

[13] J. Julian *et al.*, "Study of hydrodynamic characteristics in oscillating wave surge converter," *Jurnal Polimesin*, vol. 22, no. 2, pp. 158–164, Apr. 2024, doi: 10.30811/JPL.V22I2.4715.

[14] P. J. Roache, "Perspective: A Method for Uniform Reporting of Grid Refinement Studies," *J Fluids Eng*, vol. 116, no. 3, pp. 405–413, Sep. 1994, doi: 10.1115/1.2910291.

[15] D. Hoek, "Forced Changes Only: A New Take on the Law of Inertia," *Philos Sci*, vol. 90, no. 1, pp. 60–76, Jan. 2023, doi: 10.1017/PSA.2021.38.

[16] H. N. Nguyen, "Is the Velocity Always in Phase with the Wave Excitation Force in Constrained Optimal Control of Wave Energy Converters?," *IFAC-PapersOnLine*, vol. 56, no. 2, pp. 2632–2637, Jul. 2023, doi: 10.1016/J.IFACOL.2023.10.1352.